Received July 11, 2020, accepted July 22, 2020, date of publication July 27, 2020, date of current version August 7, 2020.

Digital Object Identifier 10.1109/ACCESS.2020.3012283

A Brain-Computer Interface Based on Multifocal SSVEPs Detected by Inter-Task-Related Component Analysis

JIABEI TANG[1], MINPENG XU[1,2,3], (Member, IEEE), ZHENG LIU[1], JINGJUAN QIAO[1], SHUANG LIU[3], SHANGUANG CHEN[1,3,4], TZYY-PING JUNG[1,3,5], (Fellow, IEEE), AND DONG MING[1,3], (Senior Member, IEEE)

[1]Department of Biomedical Engineering, School of Precision Instruments and Optoelectronics Engineering, Tianjin University, Tianjin 300072, China
[2]Tianjin Artificial Intelligence Innovation Center (TAIIC), Tianjin 300457, China
[3]Academy of Medical Engineering and Translational Medicine, Tianjin University, Tianjin 300072, China
[4]National Key Laboratory of Human Factors Engineering, China Astronaut Research and Training Center, Beijing 100094, China
[5]Swartz Center for Computational Neuroscience, University of California at San Diego, San Diego, CA 92093, USA

Corresponding authors: Minpeng Xu (minpeng.xu@tju.edu.cn) and Dong Ming (richardming@tju.edu.cn)

This work was supported in part by the National Key Research and Development Program of China under Grant 2017YFB1300300; in part by the National Natural Science Foundation of China under Grant 81925020 and Grant 61976152; and in part by the Young Elite Scientist Sponsorship Program by the China Association for Science and Technology (CAST) under Grant 2018QNRC001.

ABSTRACT Multifocal steady-state visual evoked potentials (mfSSVEPs) have been successfully applied to assess visual field loss in glaucoma. However, the potential of mfSSVEPs for command control has not been fully explored yet. It is significant to detect single-trial mfSSVEPs and establish a brain-computer interface (BCI) system. This study designed a stimulating paradigm that contains 32 targets, with each target composed of five fan-shaped flickers in a circle. The five flickers were modulated by five frequencies and formed a five-bit binary encoding system through controlling the ON/OFF state of each flicker. Twelve subjects participated in an offline and an online experiments. Inter-task-related component analysis (iTRCA) combined with a probabilistic model was proposed for target recognition. Notably, the training data needed for calibration corresponded to only six out of the 32 targets. It was found that the increasing number of flickers showed a negative impact on the mfSSVEP signal. The accuracy reached 80.9% $\pm$ 11.7% on average with a peak of 95.3% by iTRCA, which was significantly higher than that by a traditional method. The results indicate that the proposed stimulation and algorithm are effective for encoding and decoding BCI commands. Therefore, the mfSSVEP-based BCI enables the augmentation of the BCI instruction set without any burden of collecting extra training data.

INDEX TERMS Brain-computer interface (BCI), steady-state visual evoked potential (SSVEP), multifocal SSVEP (mfSSVEP), inter-task-related component analysis (iTRCA).

I. INTRODUCTION

A brain-computer interface (BCI) could measure the brain signal of users and communicate with the external devices, which can help people with motor disabilities to improve the life quality [1], [2]. Some special appliance operators such as astronauts whose movements were restricted by the environment could also benefit from the BCIs [3], [4]. Electroencephalogram (EEG) which owns the advantage of convenience, low cost, and high temporal resolution is the most welcomed brain signal for BCIs. Event-related potentials (ERPs) [5], [6], steady-state visual evoked potentials (SSVEPs) [7] and sensory motor rhythms (SMRs) [8], [9] are exemplary EEG features for BCI development. Among these features, the SSVEPs induced by repetitive stimulus at frequency above 6 Hz [10] were widely used in reactive BCIs to construct a large instruction set. As a rhythmic signal that contains the spectral components at the fundamental and harmonic stimulating frequencies, the SSVEPs possess excellent stability and high signal-to-noise ratios (SNRs), thus becoming one of the most efficient EEG features to conduct cognitive research [11], [12] or realize a high-speed

The associate editor coordinating the review of this manuscript and approving it for publication was Hasan S. Mir.

BCI system [13]. As is well known, the frequency band corresponding to high-SNR SSVEPs is narrow, thus becoming a challenge to increase the number of targets. Although several studies have proposed paradigms with high-frequency SSVEPs [14], [15], the performance could not reach the same level of low-frequency SSVEP-BCIs as the signals were weak and submerged in the background EEGs. It is worth continually exploring the potential of the golden frequency band of SSVEPs.

Recently, Nakanishi *et al.* induced multifocal SSVEPs (mfSSVEPs) with a newly developed portable platform nGoggle, in which multiple visual targets flickering at different frequencies [16], [17]. The mfSSVEP technique stimulated many areas of the retina simultaneously so that multiple kinds of responses could be detected from the EEGs. Although multifocal visual evoked potentials (mfVEPs) have been successfully applied to discriminate glaucomatous from healthy eyes by researchers [18], [19], the nGoggle combined the advantages of SSVEPs and showed a better performance in glaucoma detection. Nevertheless, this feature has not been used for BCI controls to our knowledge. If we treat the frequencies of mfSSVEPs as binary digits, i.e. given n flickers, once we decode the ON/OFF state of each flicker from the mfSSVEPs, the n flickers could encode 2^n targets. In this manner, mfSSVEPs will become an approach to expand the instruction set of SSVEP-based BCIs with much fewer frequencies than classical paradigms. In our previous study [20], a 16-target mfSSVEP-based paradigm with four frequencies encoded in a binary manner was tested and performed well. However, the targets were displayed at the center rather than in different positions of the screen so that it cannot construct a spelling system as classical SSVEPs-based systems.

In view of this, this study employed five frequencies to realize 32 targets tiled at the full screen. In order to generate the oscillation of the five frequencies stably, the flickers were arranged as fan shapes so that each flicker could be displayed in the central visual field [21]. A tailored offline stimulating experiment was designed to obtain the information of each frequency flashing at different locations of the screen. Apart from the stimulation, it is critical to find an effective method to extract the mfSSVEPs corresponding to each frequency. However, we found that the mfSSVEPs evoked by multiple flickers showed very different patterns compared with SSVEPs evoked by a single flicker. Different from the superposition of all trials in the application of glaucoma detection, the effective single-trial recognition of mfSSVEPs should be realized in a BCI controlling system. Therefore, it needs a tailored spatial filtering method for single-trial mfSSVEP extraction. Although a variety of algorithms have been successfully applied to SSVEP detection, e.g. canonical correlation analysis (CCA) [22] and its various modifications [23], minimum energy combination (MEC) [24], task-related component analysis (TRCA) [25] and so on, they were designed to extract SSVEPs under the stimulating of a single frequency, and the performance would degrade when being used to extract mfSSVEPs under simultaneous stimulating of multiple frequencies according to our preliminary tests.

Taking above issues into account, this study developed a novel inter-task-related component analysis (iTRCA) algorithm by incorporating the interclass correlation between EEGs evoked by a single flicker and all flickers into the optimizing process of the spatial filter. Besides, the intraclass correlation of a single flicker, the interclass correlation between relevant and irrelevant flickers were also transformed as covariance matrices to facilitate the optimization. In this way, the extracted inter-task-related components considered both the EEGs evoked by a single flicker and EEGs evoked by multiple flickers, thus improving the recognition performance. In the following parts, this paper introduced the experimental design, evaluated the performance of iTRCA, compared it with the conventional TRCA-based method, and analyzed the effect of the number of flickers on the mfSSVEPs.

II. METHODS

A. PARTICIPANTS

Twelve healthy volunteers (seven females) aged 21 to 27 years old participated in this study. All participants have normal or corrected normal eyesight. The Ethical Committee of Tianjin Hospital approved the experimental procedures used in this study (code: 2019YLS100). Written consent was obtained from each subject after giving a detailed explanation of the experiment.

B. STIMULUS DESIGN

Fig.1 illustrates the design of the stimulation. The participants were seated at a distance of 60 cm from a 27-inch liquid-crystal display (LCD) monitor with a refresh rate of 120 Hz. The frequency approximation approach proposed by Wang *et al.* was used to generate stimulating flickers [26]. The visual stimulus (target) used to induce mfSSVEPs comprised five fan-shaped flickers with different frequencies (11 Hz, 12 Hz, 13 Hz, 14 Hz, and 15 Hz). The five flickers form a circle stimulation area that subtended 4° of visual angle. As each flicker could be either in the ON or OFF state, the five flickers could be encoded in a 5-bit binary manner, thus generating 32 targets arranged as a 4×8 matrix (Fig.1(a)). Accordingly, the mfSSVEPs would be induced with single, double, triple, quadruple, or quintuple basic spectral components, as shown in Fig.1(c). The location of each target was specially arranged to separate the targets with the same number of flickers, which could improve the accuracy according to the results of preliminary experiments. Note that there was also a target with no flickers (the target at the lower right corner). The stimulation was developed on the MATLAB platform using the Psychtoolbox 3 [27]. Each trial started with a rest period for 1 s, followed by a flash stage for 4 s. A yellow ring would appear around the circle as a cue (Fig.1(b)). During the experiment, the participants were asked to shift their gaze to the target as soon as possible within

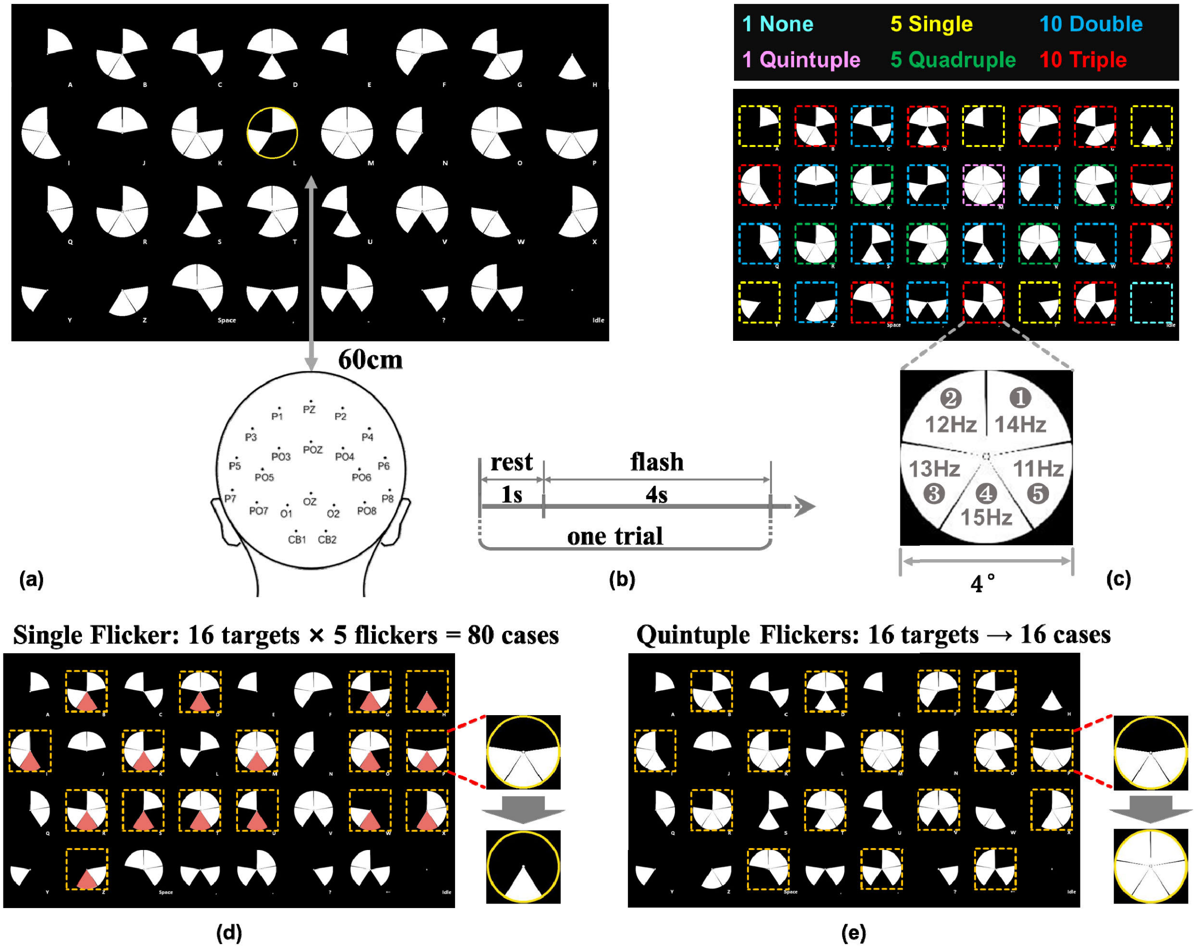

FIGURE 1. The stimulus design of the mfSSVEP-based paradigm. (a) The subjects wore a 21-channel EEG cap and seated 60 cm from the screen. The cue was presented to subjects as a yellow ring around the target. (b) Trial timing diagram of the experiment. (c) The targets with different numbers of flickers were outlined with dashed lines in different colors (the dashed lines were not displayed in the screen) and the number of targets corresponding to each number of flickers were marked above. The shapes and frequencies of the five flickers were magnified below. (d) Schematic of the single flicker stimulus corresponding to flicker 4 in the offline experiments. (e) Schematic of the quintuple flickers stimulus in the offline experiments.

the rest stage and focus on the dot displayed at the center of the circle within the flash stage.

C. EXPERIMENTAL PROCEDURE

All subjects participated in both the offline and online experiments. Twenty-four blocks were conducted in this study, including 12 offline blocks and 12 online blocks. The offline blocks were used to acquire EEGs evoked by single flicker and quintuple (all) flickers for model calibration. Theoretically, the model of the five frequencies could be trained by the data of the five targets with a single flicker. However, as each of the five flickers could be either ON or OFF as mentioned above, half of the 32 targets contain the ON state of each flicker at any given moment. Fig.1(d) illustrates the stimulating procedure by taking flicker 4 as an example. The flicker 4 was in ON state (labeled in red) at the 16 targets marked by dashed squares. Hence, the 16 targets were used to obtain information of 16 different locations from the offline data and construct a more effective model. When the 16 targets were prompted to the subject, only the flicker itself would flash (ON state) while the other four flickers were all turned off. The stimulating procedure for other flickers were conducted in the same manner. In this way, there were $16 \times 5 = 80$ cases used for single flicker stimulus evoking SSVEPs with a single frequency. As for quintuple (all) flickers, the targets with triple (10), quadruple (5), and quintuple (1) flickers were adopted and in total 16 multi-flicker targets were used in this study, as marked with dashed squares in Fig.1(e). When these targets were cued, all flickers would flash to evoke mfSSVEPs with five frequency components. In consequence, there were $80 + 16 = 96$ cases for both single and quintuple flickers in the offline experiment. Each of the 96 cases was presented twice, which led to $2 \times 96 = 192$ trials. The trials were divided into 12 blocks with 16 trials stimulating in a random sequence in each block. The subjects could take a rest after finishing a block, and begin the next block when they got enough rest according to the self-feeling. After the offline training, a classification model was built (illustrated in section II-E) for the online tests.

In online experiments, each of the 32 targets was prompted six times thus generating $6 \times 32 = 192$ trials. The trials were also divided into 12 blocks. Note that each target flashed as the pattern it is as shown in Fig.1(a) without transformation like the offline experiments. The online classification result of each trial would be reported by voice as feedback to the subjects. The subjects could also have a rest between blocks as in offline experiments. The offline and online experiments took about 45 min in total considering the resting period.

D. EEG ACQUISITION AND PREPROCESSING

The EEG data were recorded with a Neuroscan SynAmps2 amplifier and a 64-Channel Quick-Cap, with Ag/AgCl electrodes placed at standard positions of the international 10-20 system. All channels were referenced to the vertex and grounded to the prefrontal lobe between FPz and Fz during acquisition. The EEG data from twenty-one channels around the occipital area (P7, P5, P3, P1, Pz, P2, P4, P6, P8, PO7, PO5, PO3, POz, PO4, PO6, PO8, CB1, O1, Oz, O2 and CB2, see Fig.1(a)) were used for further analyses. EEG signals were band-pass filtered at 0.1-200 Hz, notch filtered at 50 Hz, sampled at 1000 Hz, and stored on the disk. In pre-processing, the data were band-pass filtered to 3-90 Hz with a 4th-order Chebyshev Type I infinite impulse response (IIR) filter and down-sampled at 250 Hz. The EEG epochs were extracted in [0.1 s, 0.1 $+t$ s] according to the onset of flashing stage, with the latency delay in the visual system defined as 0.1 s. In online experiments, $t = 4$ s, while in analysis after experiments (section III-A), t was set as 0.25 s to 4 s with an interval of 0.25 s.

E. EEG DATA ANALYSIS

1) ITRCA-BASED SPATIAL FILTER

To recognize the 32 targets with the model constructed from the offline data, this study proposed a novel spatial filtering algorithm that was termed iTRCA. For an EEG epoch $\boldsymbol{X} = (\boldsymbol{x}_1, \boldsymbol{x}_2, \cdots, \boldsymbol{x}_{N_c})^T \in \mathbb{R}^{N_c \times N_t}$, where N_c indicates the number of channels and N_t is the number of sampling points, the spatially filtering process is to get a linear sum of all the recorded channels:

$$\boldsymbol{y} = \boldsymbol{w}^T \boldsymbol{X} = \sum_{k=1}^{N_c} w_k \boldsymbol{x}_k^T \in \mathbb{R}^{1 \times N_t}. \tag{1}$$

Here, $\boldsymbol{w} = (w_1, w_2, \cdots, w_{N_c})^T$ is the spatial filter vector. It is known that the TRCA aims to maximize the reproducibility from trial to trial. However, if the spatial filters are generated from epochs of a single flicker by TRCA, the output of spatial filters may not fit the epochs of multiple flickers and result in performance degradation. The spatial filter needs to consider both the single and multiple flickers. Obviously, if the spatial filter could satisfy the two extreme cases: EEGs evoked by a single flicker and all flickers, it will be suitable for other conditions as well.

Based on the above idea, for the i-th frequency ($i = 1, 2, \ldots, N_f$, $N_f = 5$ in this study), the objective of the iTRCA spatial filter i is to maximize the correlation between epochs evoked by a single flicker i and epochs evoked by all (quintuple) flickers. The problem can be solved by inter-trial and inter-task covariance maximization. The h-th trial of EEG epoch and the estimated inter-task-related component for a single flicker i can be described as $\boldsymbol{X}_{i(h_1)}^{(S)}$ and $\boldsymbol{y}_{i(h_1)}^{(S)}$, $h_1 = 1, 2, \ldots, N_i^{(S)}$, while the h-th trial of EEG epoch and the estimated inter-task-related components for all flickers can be described as $\boldsymbol{X}_{(h_2)}^{(A)}$ and $\boldsymbol{y}_{i(h_2)}^{(A)}$, $h_2 = 1, 2, \ldots, N^{(A)}$. Then all possible combinations of trials between the two conditions are summed as

$$\begin{aligned} C_i &= \frac{1}{N_i^{(S)} N^{(A)}} \sum_{h_1=1}^{N_i^{(S)}} \sum_{h_2=1}^{N^{(A)}} \operatorname{cov}\left(\boldsymbol{y}_{i(h_1)}^{(S)}, \boldsymbol{y}_{i(h_2)}^{(A)}\right) \\ &= \frac{1}{N_i^{(S)} N^{(A)}} \sum_{h_1=1}^{N_i^{(S)}} \sum_{h_2=1}^{N^{(A)}} \boldsymbol{y}_{i(h_1)}^{(S)} \boldsymbol{y}_{i(h_2)}^{(A)T} \\ &= \frac{1}{N_i^{(S)} N^{(A)}} \sum_{h_1=1}^{N_i^{(S)}} \sum_{h_2=1}^{N^{(A)}} \left[\boldsymbol{w}_i^T \boldsymbol{X}_{i(h_1)}^{(S)}\right] \left[\boldsymbol{w}_i^T \boldsymbol{X}_{(h_2)}^{(A)}\right]^T \\ &= \boldsymbol{w}_i^T \left(\frac{1}{N_i^{(S)}} \sum_{h_1=1}^{N_i^{(S)}} \boldsymbol{X}_{i(h_1)}^{(S)}\right) \left(\frac{1}{N^{(A)}} \sum_{h_2=1}^{N^{(A)}} \boldsymbol{X}_{(h_2)}^{(A)}\right)^T \boldsymbol{w}_i \\ &= \boldsymbol{w}_i^T \bar{\boldsymbol{X}}_i^{(S)} \bar{\boldsymbol{X}}^{(A)T} \boldsymbol{w}_i \quad \rightarrow \max, \end{aligned} \tag{2}$$

where

$$\bar{\boldsymbol{X}}_i^{(S)} = \frac{1}{N_i^{(S)}} \sum_{h_1=1}^{N_i^{(S)}} \boldsymbol{X}_{i(h_1)}^{(S)} \quad \bar{\boldsymbol{X}}^{(A)} = \frac{1}{N^{(A)}} \sum_{h_2=1}^{N^{(A)}} \boldsymbol{X}_{(h_2)}^{(A)} \tag{3}$$

represent the averages across trials. To get a symmetric matrix, define

$$\boldsymbol{S}_i^{(SA)} = \bar{\boldsymbol{X}}_i^{(S)} \bar{\boldsymbol{X}}^{(A)T} + \bar{\boldsymbol{X}}^{(A)} \bar{\boldsymbol{X}}_i^{(S)T}. \tag{4}$$

In order to bound the solution, the variance of the two conditions $\boldsymbol{y}_{i(h)}^{(S)}$ and $\boldsymbol{y}_{i(h)}^{(A)}$ are constrained as

$$\operatorname{Var}(\boldsymbol{y}) = \boldsymbol{w}_i^T \boldsymbol{Q}_i \boldsymbol{w}_i = \boldsymbol{w}_i^T \left(\boldsymbol{Q}_i^{(S)} + \boldsymbol{Q}^{(A)}\right) \boldsymbol{w}_i = 1. \tag{5}$$

where

$$\boldsymbol{Q}_i^{(S)} = \frac{1}{N_i^{(S)}} \sum_{h=1}^{N_i^{(S)}} \boldsymbol{X}_{i(h)}^{(S)} \boldsymbol{X}_{i(h)}^{(S)\,T} \boldsymbol{Q}^{(A)} = \frac{1}{N^{(A)}} \sum_{h=1}^{N_i^{(A)}} \boldsymbol{X}_{(h)}^{(A)} \boldsymbol{X}_{(h)}^{(A)\,T}. \tag{6}$$

In this way, the iTRCA can be formulated as an eigenvalue problem as

$$\hat{\boldsymbol{w}}_i = \arg\max_{\boldsymbol{w}} \frac{\boldsymbol{w}_i^T \boldsymbol{S}_i^{(SA)} \boldsymbol{w}_i}{\boldsymbol{w}_i^T \boldsymbol{Q}_i \boldsymbol{w}_i}. \tag{7}$$

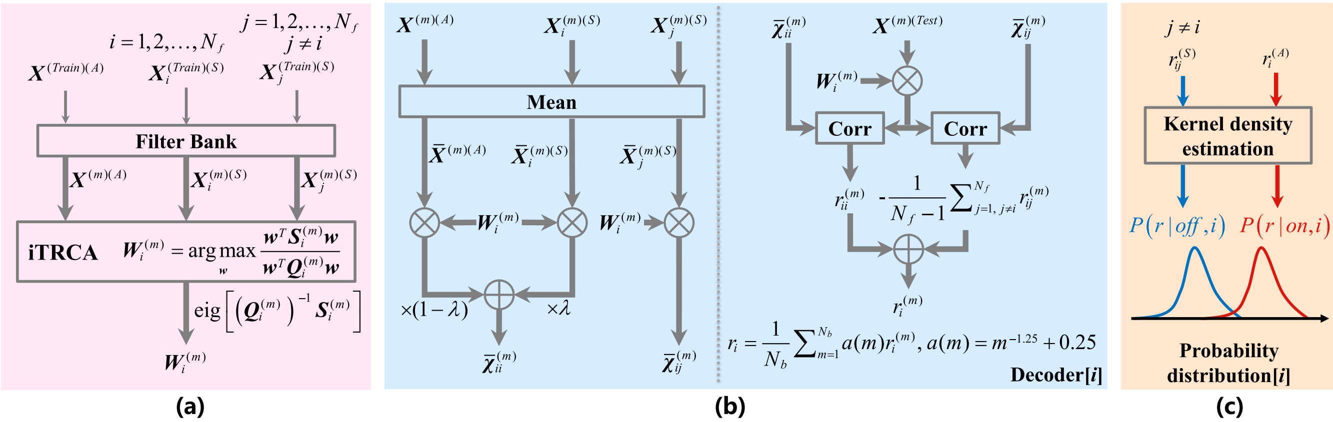

FIGURE 2. Diagrams of the modeling procedure for the i-th frequency: (A) The spatial filter generated by iTRCA, (B) the generation of template signals (left) and the calculation of correlation coefficients (right) based on the generated spatial filter, and (C) the probability distribution estimated for ON/OFF state decision.

Besides the maximization of inter-task correlation between single flicker and all flickers, some other constrains are supposed to be taken into account which may contribute to a better extraction of mfSSVEPs:

i. The maximization of inner-task correlation for a single flicker i (i.e. the matrix $\boldsymbol{S}$ in TRCA)

$$\boldsymbol{S}_{ii}^{(SS)} = \frac{1}{N_i^{(S)}\left(N_i^{(S)}-1\right)} \sum_{\substack{h_1=1,h_2=1\\ h_1\neq h_2}}^{N_i^{(S)}} \boldsymbol{X}_{i(h_1)}^{(S)} \boldsymbol{X}_{i(h_2)}^{(S)T} = \frac{1}{N_i^{(S)}\left(N_i^{(S)}-1\right)} \times \left[\sum_{h_1=1,h_2=1}^{N_i^{(S)}} \boldsymbol{X}_{i(h_1)}^{(S)} \boldsymbol{X}_{i(h_2)}^{(S)T} - \sum_{\substack{h_1=1,h_2=1\\ h_1=h_2}}^{N_i^{(S)}} \boldsymbol{X}_{i(h_1)}^{(S)} \boldsymbol{X}_{i(h_2)}^{(S)T}\right] = \frac{1}{N_i^{(S)}-1}\left[N_i^{(S)} \cdot \bar{\boldsymbol{X}}_i^{(S)} \bar{\boldsymbol{X}}_i^{(S)\,T} - \boldsymbol{Q}_i^{(S)}\right] \quad (8)$$

ii. The minimization of inter-task correlation between a single flicker j ($j \neq i$) (unrelated frequencies for frequency i) and a single flicker i

$$-\boldsymbol{S}_{ij}^{(SS)} = -\left[\bar{\boldsymbol{X}}_i^{(S)\,T} \bar{\boldsymbol{X}}_j^{(S)} + \bar{\boldsymbol{X}}_j^{(S)\,T} \bar{\boldsymbol{X}}_i^{(S)}\right]. \quad (9)$$

iii. The minimization of inter-task correlation between a single flicker j ($j \neq i$) and all flickers

$$-\boldsymbol{S}_j^{(SA)} = -\left[\bar{\boldsymbol{X}}_j^{(S)} \bar{\boldsymbol{X}}^{(A)\,T} + \bar{\boldsymbol{X}}^{(A)} \bar{\boldsymbol{X}}_j^{(S)\,T}\right]. \quad (10)$$

Then the matrix $\boldsymbol{S}_i^{(SA)}$ can be optimized as $\boldsymbol{S}_i$

$$\boldsymbol{S}_i = \boldsymbol{S}_i^{(SA)} - \frac{1}{N_f-1}\sum_{j=1,j\neq i}^{N_f} \boldsymbol{S}_j^{(SA)} + \boldsymbol{S}_{ii}^{(SS)} - \frac{1}{N_f-1}\sum_{j=1,j\neq i}^{N_f} \boldsymbol{S}_{ij}^{(SS)}, \quad (11)$$

and the matrix $\boldsymbol{Q}_i$ can be modified accordingly as

$$\boldsymbol{Q}_i = \frac{1}{4}\left(2\boldsymbol{Q}_i^{(S)} + \boldsymbol{Q}_i^{(A)} + \frac{1}{N_f-1}\sum_{j=1,j\neq i}^{N_f} \boldsymbol{Q}_j^{(S)}\right). \quad (12)$$

In this way, the spatial filter $\hat{\boldsymbol{w}}_i$ can be derived from (7) as the eigenvectors of $\boldsymbol{Q}_i^{-1}\boldsymbol{S}_i$ by solving the eigenvalue decomposition problem. In this paper, the performance of iTRCA and classical TRCA methods was compared below.

2) MODELING PROCEDURE

Fig.2 illustrates the procedure of model construction with the offline data for the i-thfrequency. The data from 21 channels were fed into a filter bank to decompose the EEGs into sub-band waves to extract information embedded in the harmonic components. The lower and upper cut-off frequencies of the m-th sub-band were set to $(1 + m \times 9)$Hz and 88 Hz, respectively ($m = 1, 2$). This study used the zero-phase Chebyshev Type I infinite impulse response (IIR) filters. As presented in Fig.2(a), iTRCA spatial filters $\boldsymbol{W}_i^{(m)}$ $(i = 1, 2, \ldots, N_f)$ were firstly constructed for the m-th sub-band using the offline data.

The left panel of Fig.2(b) shows the generation of template signal for mfSSVEP recognition. Firstly, the data of the single flicker and all flickers were both considered so that the template involves information from both the single and multiple flickers. Hence, the averages across trials of the two groups $\bar{\boldsymbol{X}}^{(m)(A)}$ and $\bar{\boldsymbol{X}}_i^{(m)(S)}$ were multiplied by $\boldsymbol{W}_i^{(m)}$ and summed with a weight λ (0.85 in this study) to get the templates $\bar{\boldsymbol{\chi}}_{ii}^{(m)}$. Besides the $\bar{\boldsymbol{\chi}}_{ii}^{(m)}$ that represents the positive correlation, if the data of other frequencies $\bar{\boldsymbol{X}}_j^{(m)(S)}$ $(j = 1, 2, \ldots, N_f,\ j \neq i)$ were spatially filtered by $\boldsymbol{W}_i^{(m)}$, the generated templates $\bar{\boldsymbol{\chi}}_{ij}^{(m)}$ would present a negative correlation with the i-thfrequency. It makes sense to consider the negative correlation templates that may help to improve the separability between different frequencies.

The right panel of Fig.2(b) displays the calculating procedure of correlation coefficients as the output of Decoder[i]. For the testing EEG epoch $\boldsymbol{X}^{(Test)(m)}$, the Pearson correlation coefficients with positive templates $\bar{\boldsymbol{\chi}}_{ii}^{(m)}$and negative templates $\bar{\boldsymbol{\chi}}_{ij}^{(m)}$ were calculated as $r_{ii}^{(m)}$ and $r_{ij}^{(m)}$ after the spatially

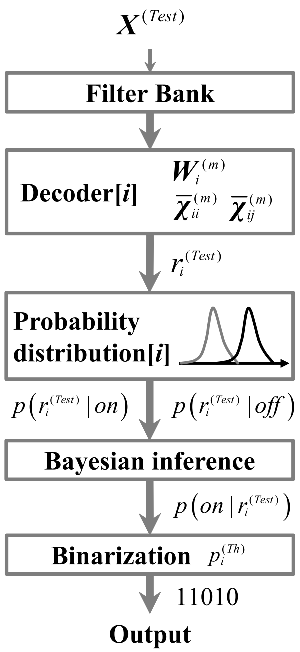

FIGURE 3. Flowchart of online recognition for the i-th frequency.

filtering procedure. The final coefficients were defined as the difference values of the positive and negative correlation coefficients:

$$r_i^{(m)} = r_{ii}^{(m)} - \frac{1}{N_f - 1} \sum_{j=1,\, j\neq i}^{N_f} r_{ij}^{(m)}. \tag{13}$$

The output coefficients r_i were calculated by a weighted mean of the coefficients corresponding to all sub-bands. In order to decode the ON/OFF state of each flicker so as to obtain the final result, the probability density functions (pdfs) of each flicker's ON/OFF states were derived from the offline data. Fig.2(c) depicts the generating procedure of the pdfs. If the data evoked by all flickers were fed into the Decoder[i], we would obtain correlation coefficients $r_i^{(A)}$. The pdfs $P(r|on, i)$ for the ON state were then generated by Gaussian kernel density estimation using $r_i^{(A)}$. If the data evoked by the j-th ($j = 1, 2, \ldots N_f$, $j \neq i$) single flicker were fed into the Decoder[i], we would obtain correlation coefficients $r_{ij}^{(S)}$. The pdfs $P(r|off, i)$ for the OFF state were then generated using $r_{ij}^{(S)}$. The correlation coefficients used for generating probability distribution were calculated using the offline data with a 16-fold cross-validation method.

3) ONLINE RECOGNITION PROCEDURE

Fig.3 shows the procedure of online recognition. For a testing trial $\boldsymbol{X}^{(Test)}$ in the online blocks, the preprocessed data were decomposed by the filter bank and then fed into Decoder[i] to compute correlation coefficients $r_i^{(Test)}$. Then the probability of ON/OFF state: $p\left(r_i^{(Test)}|on\right)$ and $p\left(r_i^{(Test)}|off\right)$ could be obtained through Probability distribution[i]. The posterior probability $p\left(on|r_i^{(Test)}\right)$ for the i-th frequency could be obtained by the Bayesian inference [28], [29]:

$$p\left(on|r_i^{(Test)}\right) = \frac{p(on)p\left(r_i^{(Test)}|on\right)}{p(on)p\left(r_i^{(Test)}|on\right) + p(off)p\left(r_i^{(Test)}|off\right)}, \tag{14}$$

in which the $p(on)$ and $p(off)$ were prior probabilities and set as $p(on) = p(off) = 0.5$. The result $p\left(on|r_i^{(Test)}\right)$ was then binarized to 1 or 0 to generate the final 5-bit binary output according to the threshold $p_i^{(Th)}$. The thresholds were optimized for every subject according to the distance between pdfs $P(r|off, i)$and $P(r|on, i)$ in this study. If the two curves live far from each other, it would be easier to differentiate the on or off state, and the thresholds were set lower. If the two curves stay close to each other, the threshold should be conservative and set to a higher value.

4) POWER SPECTRUM AND SNR OF MFSSVEPS

The power spectrums and SNRs of mfSSVEP components were analyzed using the 4 s epochs from the online experiment. Considering the amplitude spectrum $y(f)$ calculated by the 500-point fast Fourier transform (FFT), the power spectrum $P(f)$ was defined as $y^2(f)$. The SNR in decibels (dB) was defined as the ratio of $y(f)$ to the mean value of the four neighboring frequencies considering the 500-point FFT [13]:

$$\mathrm{SNR}(f) = 20 \log_{10} \frac{y(f)}{\frac{1}{4}\sum_{k=1}^{2}\left[y(f - 0.5\times k) + y(f + 0.5\times k)\right]}. \tag{15}$$

For each flicker, the power spectrum and SNR were estimated by averaging across trials and subjects.

III. RESULTS

A. PERFORMANCE OF MFSSVEP-BASED BCI

The online data were further analyzed after the experiment. Fig.4 and Table.1 show the performance analysis of the online data with the model constructed from the offline data. For the data length of 4 s which was used for online recognition in the experiments, the mean accuracy of the iTRCA-based method across all subjects was 80.9% ± 11.7% (max 95.3%), while the classical TRCA-based method showed 70.4% ± 16.3% (max 93.2%). In the offline analysis, the accuracies of the iTRCA spatial filter were significantly higher than those of the TRCA for most of the data lengths (Wilcoxon signed rank test, $p < 0.01$), as shown in Fig.4. We also calculated the putative information transfer rates (ITRs) with different data length using the common method [23]:

$$\mathrm{ITR} = \left[\log_2 N + P\log_2 P + (1-P)\log_2 \frac{1-P}{N-1}\right] \times \frac{60}{T}, \tag{16}$$

where $N = 32$ is the number of commands, P is the accuracy and T is the consuming time for each trial which includes the

TABLE 1. **The highest ITRs of all subjects in the offline analysis.**

Subject	TRCA			iTRCA		
	Length (s)	Accuracy (%)	ITR (bits/min)	Length (s)	Accuracy (%)	ITR (bits/min)
1	0.75	52.6	132.3	0.75	**55.7**	**145.3**
2	2.00	57.8	57.8	**1.75**	54.2	**59.5**
3	1.50	33.8	32.0	2.25	**55.2**	**47.7**
4	2.00	44.8	38.2	2.00	**53.7**	**51.2**
5	2.25	52.1	43.4	**1.75**	51.6	**54.9**
6	2.00	67.2	73.8	**1.50**	64.6	**92.3**
7	0.75	45.3	103.8	1.75	**82.8**	**119.5**
8	2.25	77.1	82.3	2.25	**82.8**	**93.0**
9	2.25	44.3	33.3	2.75	**58.3**	**42.7**
10	1.50	49.5	59.9	1.50	**50.5**	**62.0**
11	1.00	54.2	104.1	1.50	**71.4**	**108.7**
12	1.00	52.6	99.2	1.00	**77.6**	**187.4**
Ave±Std	-	52.6±11.2	71.7±32.9	-	**63.2±12.3**	**88.7±45.0**

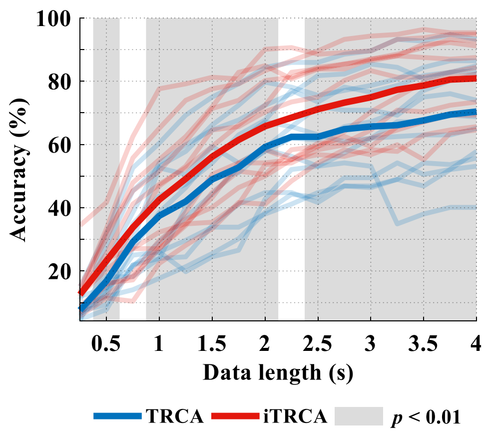

FIGURE 4. **Comparison of recognition accuracies based on TRCA and iTRCA spatial filters. Each line with light color represents one subject and the line with deep color represents the average. The grey shading shows the significance of difference between the accuracies of two spatial filters (Wilcoxon signed rank test).**

1-second interval between two successive trials. Table 1 listed the highest ITR of each subject with the corresponding data length and accuracy. The average of ITRs for iTRCA was 88.7 ± 45.0 bits/min, which is significantly higher than that for TRCA (71.7 ± 32.9 bits/min, $p = 4.88 \times 10^{-4}$). The improvement of ITRs was due to the higher accuracies or shorter data length (marked in boldface). Specifically, the highest ITR reached 187.4 bits/min with 1 s data.

B. COMPARISON OF SNRS BETWEEN TRCA AND ITRCA

The top row of Fig.5 shows the average SNR spectrums of the spatially filtered EEG data that were evoked by quintuple flickers. In view of the harmonic effect of SSVEPs, the harmonic components were also marked out. For related frequencies of each flicker (e.g. 12 Hz and its harmonics for Flicker 2), iTRCA obtained similar or higher SNRs than those of TRCA (red vs blue triangles in the figure). Besides, the unrelated frequencies for each flicker (e.g. 11, 13, 14, 15 Hz and their harmonics for Flicker 2) showed lower SNRs for iTRCA than those for TRCA (red vs blue squares in the figure).

To further evaluate the effect of two spatial filters on SNRs quantitatively, the key frequencies in the SNR spectrums (i.e. the triangles and squares) were averaged and shown in the lower row of Fig.4. For the five flickers, the figure shows that the SNRs of unrelated frequencies filtered by iTRCA were significantly lower than those by TRCA, while the SNRs of related frequencies did not show significant differences except for Flicker 3. In addition, compared to related frequencies, unrelated frequencies presented significantly lower SNRs for four flickers (11, 12, 13, 15 Hz) by iTRCA, whereas only two flickers (12, 15 Hz) had significantly lower SNRs by TRCA.

C. THE IMPACT OF THE NUMBER OF FLICKERS

Fig.6 shows the recognition accuracies for targets with 1-4 flickers, respectively. As the number of targets changes with the number of flickers (see Fig.1(c)), the targets were divided into two subgraphs to make a fair comparison, i.e. the accuracies of the group with the same number of targets were compared in the same subgraph. In Fig.6(a), the accuracies of single-flicker targets had higher accuracies than those of the quadruple flickers and the difference was statistically significant when the data length was shorter than 2.7 s. The accuracies of double-flicker targets were significantly higher than those of triple-flicker targets at all lengths of data (Fig.6(b)).

In order to compare the energy distribution corresponding to different numbers of flickers, we calculated the power spectrum of each electrode for each target through FFT. The power of fundamental, second, and third harmonics of each flicker (frequency) was then extracted and summed. These data could be categorized into 5 (flicker numbers) × 5 (frequencies) = 25 groups. For example, the target at the 2^{nd} row, 8^{th} column contains 3 flickers (Flicker 3, 4, and 5), the frequencies of which were 13 Hz, 15Hz, and 11 Hz. Therefore, the summed power of 13/26/39 Hz was categorized into the group of triple flickers & 13 Hz, the summed power of 15/30/45 Hz was categorized into the group of triple flickers & 15 Hz, and the summed power of 11/22/33 Hz was categorized into the group of triple flickers & 11 Hz. In this

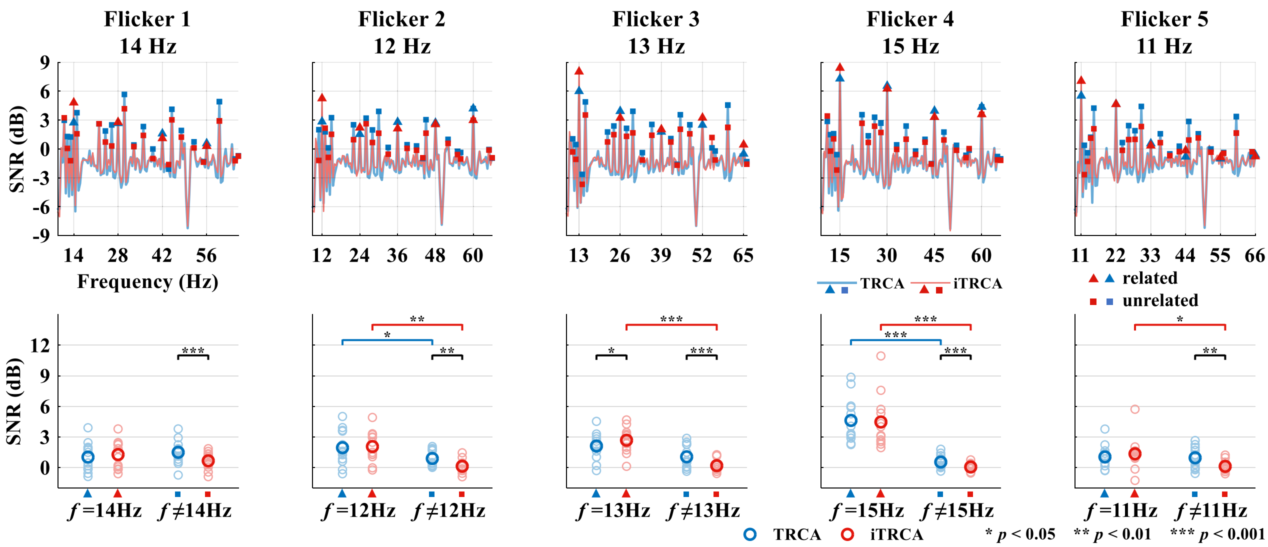

FIGURE 5. (Upper row) Average SNR spectrums of EEG data spatially filtered by TRCA and iTRCA under quintuple flickers stimulating across all trials and subjects. The triangles represent the SNRs of the related frequencies of the current flicker, while the squares represent the unrelated frequencies, i.e. the related frequencies of other flickers. (Lower row) The average of related and unrelated frequencies. The little circles with light color represent all subjects and the large circles with deep color represent the average across all subjects. The numbers of "*" indicate the significance of difference (Wilcoxon signed rank test).

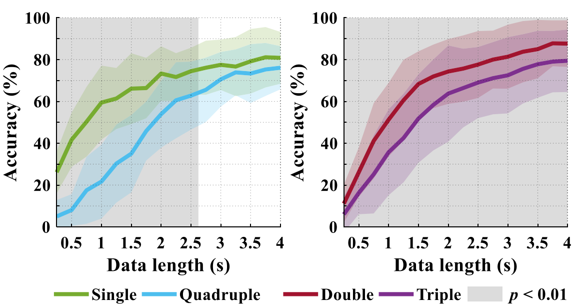

FIGURE 6. Recognition accuracies corresponding to targets with different numbers of flickers: the five targets with a single flicker and the five targets with quadruple flickers (left), as well as the ten targets with double flickers and the ten targets with triple flickers (right). The grey shading shows the significance of the differences (Wilcoxon signed rank test).

way, we could obtain 25 groups of power data after processing all the targets. The power data were averaged within each group and then averaged for all subjects. Fig.7 shows the distribution of the power at all electrodes. The topographies qualitatively showed that the power spectrum of each frequency declined with the number of flickers increased. Afterward, the power of each electrode was compared between multiple and single flickers using Wilcoxon signed rank test and the significance was marked with a cross. The power was strongest when there was only one flicker flashing (top row in Fig.7). For double flickers, few electrodes showed significant power decline compared with a single flicker. However, more electrodes presented significantly weaker power when three, four, or five flickers flashed at the same time. The right-most column represents the total power of frequencies between 0-50 Hz. The five topographies exhibited similar strength and distribution, and no significance was found between the power of a single flicker and multiple flickers.

IV. DISCUSSION

Researchers have been focusing on expanding the BCI instruction number to broaden the applications of BCIs in recent years. It is known that reactive BCIs are widely adopted to generate a large instruction set. The coding strategy of reactive BCIs can be grouped into five schemes [30]: time division multiple access (TDMA), frequency division multiple access (FDMA), code division multiple access (CDMA), space division multiple access (SDMA), and hybrid multiple access (HMA) according to the telecommunication technology. As typical FDMA systems, SSVEP-based BCIs are widely used because of their high ITRs as a consequence of unremitting efforts on the stimulation and decoding algorithms. However, the limited frequency band of high-SNR SSVEPs prevents the enlargement of their instruction set. A number of coding strategies have been proposed to overcome the restriction of frequencies. For example, Chen *et al.* introduced intermodulation frequencies to SSVEP stimulation and realized nine targets with one main frequency and nine additional modulation frequencies [31]. In recent high speed SSVEP-BCI systems, a joint frequency-phase modulation (JFPM) method greatly improved the separability between targets thus achieving high performance [32]. Thanks to the JFPM stimulation, the SSVEP-based BCIs have been continuously breaking the ITR records [33], [34] and derived a variety of applications [35], [36]. Moreover, hybrid coding that combines other EEG features such as ERPs is also a promising approach to increase the command number, as plenty of researchers have demonstrated its

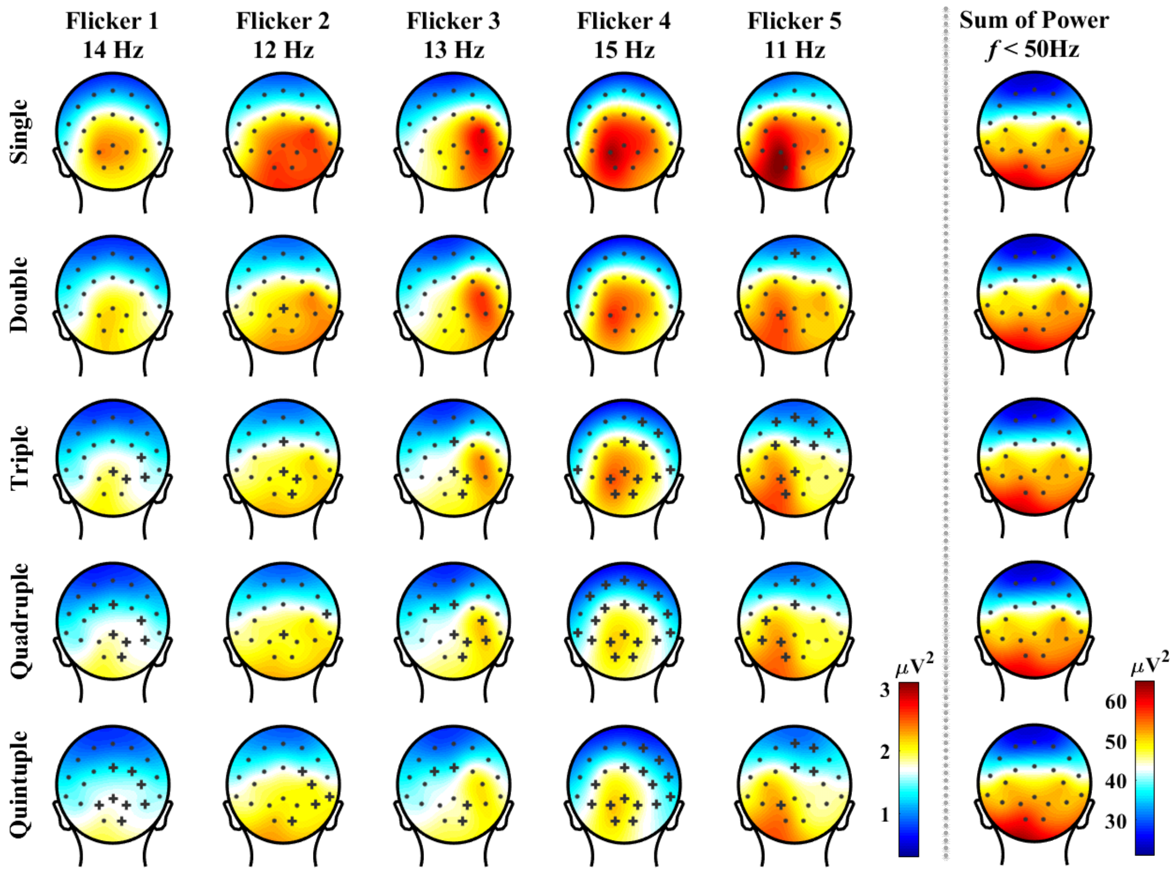

FIGURE 7. The average spectral topographies across all subjects under different numbers of flickers. The topographies were observed from the occipital direction for comprehensibility. Each row represents one group and each column represents one frequency, while the right-most column represents the summation of power for frequencies < 50 Hz. The "+" indicates the electrode at which the power was significantly lower than that of a single flicker in the uppermost row (Wilcoxon signed rank test, $p < 0.01$).

performance [37]–[40]. Different from the above strategies, this study explored the potential of mfSSVEPs to encode a 32-target BCI system with five frequencies. In order to induce stronger mfSSVEPs, the shape of the stimulus and the locations of the 32 targets were designed elaborately, as shown in Fig.1(c). What's more, the offline calibration experiment was also optimized to make the raw EEG data containing all possible locations of each flicker. The resultant accuracies and SNRs showed that the mfSSVEPs containing five frequencies were reliably evoked by the stimuli. It should be noted that the target at the bottom right corner with none flicker is a special instruction that represents an idle state. Hence the proposed BCI system could realize the asynchronous function as well.

For SSVEP-BCIs, a crucial step in the decoding algorithm is the spatial filtering procedure. Many spatial filters were proposed in previous studies and produced excellent performance in online tests, especially for TRCA [25]. It is known that TRCA extracts the task-related components by summing all covariances (correlations) of trial pairs inside one class and performing the eigenvalue decomposition. Nevertheless, the mfSSVEPs were evoked by more than one frequency, which complicate the EEG pattern. The classical TRCA spatial filter is optimized by the EEGs evoked by only one frequency, thus causing the mismatching between the model and the EEGs evoked by different numbers of flickers in consequence. It is necessary to design a novel spatial filter that can address both the single and multiple flickers. Hence, this study proposed a novel iTRCA spatial filter. Different from TRCA, four factors were taken into account as four covariance matrices in iTRCA: maximizing the interclass correlation between the EEGs of current flicker and all flickers ($\boldsymbol{S}_i^{(SA)}$), minimizing the interclass correlation between the EEGs of other flickers and all flickers ($-\boldsymbol{S}_j^{(SA)}$), maximizing the intraclass correlation within the EEGs of current flicker ($\boldsymbol{S}_{ii}^{(SS)}$), minimizing the interclass correlation between the EEGs of current flicker and other flickers ($-\boldsymbol{S}_{ij}^{(SS)}$). The SNRs in Fig.5 and the accuracies in Fig.4 proved that the generated iTRCA spatial filter for each flicker suppressed the irrelevant signals evoked by other flickers more effectively than the TRCA spatial filter. The methodology of iTRCA will also help extract common information in multitasking researches.

As newly applied EEG features, the characters of mfSSVEPs have not been fully understood yet. This study analyzed the variation of mfSSVEPs with the numbers of flickers. The accuracies in Fig.6 demonstrate that the number of flickers had a negative influence on the performance of mfSSVEP-based BCI. Fig.7 provides a qualitative analysis of this effect from the perspective of the power spectrum. The results suggested that the total energy supplied to the brain tends to be constant and allocated according to needs. A previous study proposed that the number of neurons that can be activated was inversely proportional to the average discharge rate of active neurons [41]. This mechanism ensures the energy consumption of the brain remains at a relatively low level. If more competitive stimuli are flashing simultaneously, the entire energy needs to be allocated to more frequencies so that each frequency will acquire less power. In future work, it is of vital importance to master the characters of mfSSVEPs in depth, and develop a more robust decoding algorithm to benefit the instruction expanding. Besides, Fig.6 also shows that the lateral visual stimuli used in this study caused the contralateral power distribution of mfSSVEPs. This is in accordance with the retinotopic mapping theory mentioned in previous studies [42], [43].

V. CONCLUSION

This study verified the feasibility of utilizing mfSSVEPs to encode a multi-target BCI system. An mfSSVEP-based BCI speller with five binary-coded flickers was developed and a novel iTRCA spatial filter was designed to extract the related components of each flicker. The online results demonstrated the effectiveness of the proposed paradigm and the algorithm. With continual optimization, the proposed paradigm is promising to realize a larger number of commands with fewer frequencies and less calibration time.

ACKNOWLEDGMENT

The authors sincerely thank all the participants for their voluntary participation and thank the reviewers as well as editors for their precious suggestions and comments.

REFERENCES

[1] J. Wolpaw and E. W. Wolpaw, *Brain-Computer Interfaces: Principles and Practice*. Oxford, U.K.: Oxford Univ. Press, 2012.

[2] M. Velliste, S. Perel, M. C. Spalding, A. S. Whitford, and A. B. Schwartz, "Cortical control of a prosthetic arm for self-feeding," *Nature*, vol. 453, no. 7198, p. 1098, 2008.

[3] C. de Negueruela, M. Broschart, C. Menon, and J. del R. Millán, "Brain–computer interfaces for space applications," *Pers. Ubiquitous Comput.*, vol. 15, no. 5, pp. 527–537, Jun. 2011, doi: 10.1007/s00779-010-0322-8.

[4] S. Chen, J. Jiang, J. Tang, X. Jiao, H. Qi, Y. Cao, C. Wang, and D. Ming, "An experimental study on usability of brain-computer interaction technology in human spaceflight," in *Augmented Cognition. Enhancing Cognition and Behavior in Complex Human Environments*. Cham, Switzerland: Springer, 2017, pp. 301–312.

[5] M. Xu, X. Xiao, Y. Wang, H. Qi, T.-P. Jung, and D. Ming, "A brain–computer interface based on miniature-event-related potentials induced by very small lateral visual stimuli," *IEEE Trans. Biomed. Eng.*, vol. 65, no. 5, pp. 1166–1175, May 2018, doi: 10.1109/TBME.2018.2799661.

[6] X. Xiao, M. Xu, J. Jin, Y. Wang, T.-P. Jung, and D. Ming, "Discriminative canonical pattern matching for single-trial classification of ERP components," *IEEE Trans. Biomed. Eng.*, vol. 67, no. 8, pp. 2266–2275, Aug. 2020, doi: 10.1109/TBME.2019.2958641.

[7] M. Nakanishi, Y. Wang, Y. T. Wang, Y. Mitsukura, and T. P. Jung, "A high-speed brain speller using steady-state visual evoked potentials," (in English), *Int. J. Neural Syst.*, vol. 24, no. 6, Sep. 2014, Art. no. 1450019, doi: 10.1142/S0129065714500191.

[8] L. Xu, M. Xu, Y. Ke, X. An, S. Liu, and D. Ming, "Cross-dataset variability problem in EEG decoding with deep learning," *Frontiers Hum. Neurosci.*, vol. 14, p. 103, Apr. 2020, doi: 10.3389/fnhum.2020.00103.

[9] K. Wang, M. Xu, Y. Wang, S. Zhang, L. Chen, and D. Ming, "Enhance decoding of pre-movement EEG patterns for brain–computer interfaces," *J. Neural Eng.*, vol. 17, no. 1, Jan. 2020, Art. no. 016033, doi: 10.1088/1741-2552/ab598f.

[10] F. B. Vialatte, M. Maurice, J. Dauwels, and A. Cichocki, "Steady-state visually evoked potentials: Focus on essential paradigms and future perspectives," *Prog. Neurobiol.*, vol. 90, no. 4, pp. 418–438, Apr. 2010, doi: 10.1016/j.pneurobio.2009.11.005.

[11] K. A. Ellis, R. B. Silberstein, and P. J. Nathan, "Exploring the temporal dynamics of the spatial working memory n-back task using steady state visual evoked potentials (SSVEP)," *NeuroImage*, vol. 31, no. 4, pp. 1741–1751, Jul. 2006.

[12] M. Xu, Y. Jia, H. Qi, Y. Hu, F. He, X. Zhao, P. Zhou, L. Zhang, B. Wan, W. Gao, and D. Ming, "Use of a steady-state baseline to address evoked vs. Oscillation models of visual evoked potential origin," *NeuroImage*, vol. 134, pp. 204–212, Jul. 2016.

[13] X. Chen, Y. Wang, S. Gao, T.-P. Jung, and X. Gao, "Filter bank canonical correlation analysis for implementing a high-speed SSVEP-based brain–computer interface," *J. Neural Eng.*, vol. 12, no. 4, Aug. 2015, Art. no. 046008.

[14] X. Chen, B. Zhao, Y. Wang, and X. Gao, "Combination of high-frequency SSVEP-based BCI and computer vision for controlling a robotic arm," *J. Neural Eng.*, vol. 16, no. 2, Apr. 2019, Art. no. 026012, doi: 10.1088/1741-2552/aaf594.

[15] A. Chabuda, P. Durka, and J. Zygierewicz, "High frequency SSVEP-BCI with hardware stimuli control and phase-synchronized comb filter," *IEEE Trans. Neural Syst. Rehabil. Eng.*, vol. 26, no. 2, pp. 344–352, Feb. 2018, doi: 10.1109/TNSRE.2017.2734164.

[16] J. K. Zao, Y.-Y. Chien, F.-C. Lin, Y.-T. Wang, M. Nakanishi, F. A. Medeiros, T.-P. Jung, and Y.-P. Huang, "37-4: Invited paper: Intelligent virtual-reality head-mounted displays with brain monitoring and visual function assessment," in *Proc. SID Symp. Dig. Tech. Papers*, 2018, vol. 49, no. 1, pp. 475–478.

[17] M. Nakanishi, Y.-T. Wang, T.-P. Jung, J. K. Zao, Y.-Y. Chien, A. Diniz-Filho, F. B. Daga, Y.-P. Lin, Y. Wang, and F. A. Medeiros, "Detecting glaucoma with a portable brain-computer interface for objective assessment of visual function loss," *JAMA Ophthalmol.*, vol. 135, no. 6, p. 550, Jun. 2017.

[18] F. Sabeti, A. C. James, C. F. Carle, R. W. Essex, A. Bell, and T. Maddess, "Comparing multifocal pupillographic objective perimetry (mfPOP) and multifocal visual evoked potentials (mfVEP) in retinal diseases," *Sci. Rep.*, vol. 7, no. 1, p. 45847, Apr. 2017, doi: 10.1038/srep45847.

[19] D. C. Hood, P. Thienprasiddhi, V. C. Greenstein, B. J. Winn, N. Ohri, J. M. Liebmann, and R. Ritch, "Detecting early to mild glaucomatous damage: A comparison of the multifocal VEP and automated perimetry," *Investigative Ophthalmol. Vis. Sci.*, vol. 45, no. 2, pp. 492–498, 2004, doi: 10.1167/iovs.03-0602.

[20] J. Tang, M. Xu, Z. Liu, J. Meng, S. Chen, and D. Ming, "A multifocal SSVEPs-based brain-computer interface with less calibration time*," in *Proc. 41st Annu. Int. Conf. IEEE Eng. Med. Biol. Soc. (EMBC)*, Jul. 2019, pp. 5975–5978, doi: 10.1109/EMBC.2019.8857450.

[21] E. L. Schwartz, "Spatial mapping in the primate sensory projection: Analytic structure and relevance to perception," *Biol. Cybern.*, vol. 25, no. 4, pp. 181–194, Dec. 1977, doi: 10.1007/BF01885636.

[22] Z. Lin, C. Zhang, W. Wu, and X. Gao, "Frequency recognition based on canonical correlation analysis for SSVEP-based BCIs," *IEEE Trans. Biomed. Eng.*, vol. 53, no. 12, pp. 2610–2614, Dec. 2006.

[23] X. Chen, Y. Wang, M. Nakanishi, X. Gao, T.-P. Jung, and S. Gao, "High-speed spelling with a noninvasive brain-computer interface," *Proc. Nat. Acad. Sci. USA*, vol. 112, no. 44, pp. E6058–E6067, 2015.

[24] O. Friman, I. Volosyak, and A. Graser, "Multiple channel detection of steady-state visual evoked potentials for brain-computer interfaces," *IEEE Trans. Biomed. Eng.*, vol. 54, no. 4, pp. 742–750, Apr. 2007, doi: 10.1109/TBME.2006.889160.
[25] M. Nakanishi, Y. Wang, X. Chen, Y.-T. Wang, X. Gao, and T.-P. Jung, "Enhancing detection of SSVEPs for a high-speed brain speller using task-related component analysis," *IEEE Trans. Biomed. Eng.*, vol. 65, no. 1, pp. 104–112, Jan. 2018.
[26] Y. Wang, Y. T. Wang, and T. P. Jung, "Visual stimulus design for high-rate SSVEP BCI," *Electron. Lett.*, vol. 46, no. 15, pp. 1057–1058, 2010, doi: 10.1049/el.2010.0923.
[27] D. H. Brainard, "The psychophysics toolbox," *Spatial Vis.*, vol. 10, no. 4, pp. 433–436, 1997.
[28] H. Zhang, C. Guan, and C. Wang, "Asynchronous P300-based brain-computer interfaces: A computational approach with statistical models," *IEEE Trans. Biomed. Eng.*, vol. 55, no. 6, pp. 1754–1763, Jun. 2008.
[29] B. O. Mainsah, L. M. Collins, K. A. Colwell, E. W. Sellers, D. B. Ryan, K. Caves, and C. S. Throckmorton, "Increasing BCI communication rates with dynamic stopping towards more practical use: An ALS study," *J. Neural Eng.*, vol. 12, no. 1, Feb. 2015, Art. no. 016013.
[30] S. Gao, Y. Wang, X. Gao, and B. Hong, "Visual and auditory brain–computer interfaces," *IEEE Trans. Bio-Med. Eng.*, vol. 61, no. 5, pp. 1436–1447, May 2014, doi: 10.1109/TBME.2014.2300164.
[31] X. Chen, Z. Chen, S. Gao, and X. Gao, "Brain–computer interface based on intermodulation frequency," *J. Neural Eng.*, vol. 10, no. 6, Dec. 2013, Art. no. 066009.
[32] X. Chen, Y. Wang, M. Nakanishi, T.-P. Jung, and X. Gao, "Hybrid frequency and phase coding for a high-speed SSVEP-based BCI speller," in *Proc. 36th Annu. Int. Conf. IEEE Eng. Med. Biol. Soc.*, Aug. 2014, pp. 3993–3996, doi: 10.1109/EMBC.2014.6944499.
[33] K. Lin, S. Gao, and X. Gao, "Boosting the information transfer rate of an SSVEP-BCI system using maximal-phase-locking value and minimal-distance spatial filter banks," *Tsinghua Sci. Technol.*, vol. 24, no. 3, pp. 262–270, Jun. 2019, doi: 10.26599/TST.2018.9010010.
[34] J. Jiang, E. Yin, C. Wang, M. Xu, and D. Ming, "Incorporation of dynamic stopping strategy into the high-speed SSVEP-based BCIs," *J. Neural Eng.*, vol. 15, no. 4, Aug. 2018, Art. no. 046025.
[35] Y.-T. Wang, M. Nakanishi, S. L. Kappel, P. Kidmose, D. P. Mandic, Y. Wang, C.-K. Cheng, and T.-P. Jung, "Developing an online steady-state visual evoked potential-based brain-computer interface system using EarEEG," in *Proc. 37th Annu. Int. Conf. IEEE Eng. Med. Biol. Soc. (EMBC)*, Aug. 2015, pp. 2271–2274.
[36] Y. Ke, P. Liu, X. An, X. Song, and D. Ming, "An online SSVEP-BCI system in an optical see-through augmented reality environment," *J. Neural Eng.*, vol. 17, no. 1, Feb. 2020, Art. no. 016066, doi: 10.1088/1741-2552/ab4dc6.
[37] M. Xu, H. Qi, B. Wan, T. Yin, Z. Liu, and D. Ming, "A hybrid BCI speller paradigm combining P300 potential and the SSVEP blocking feature," *J. Neural Eng.*, vol. 10, no. 2, Apr. 2013, Art. no. 026001, doi: 10.1088/1741-2560/10/2/026001.
[38] E. Yin, Z. Zhou, J. Jiang, F. Chen, Y. Liu, and D. Hu, "A speedy hybrid BCI spelling approach combining P300 and SSVEP," *IEEE Trans. Biomed. Eng.*, vol. 61, no. 2, pp. 473–483, Feb. 2014, doi: 10.1109/TBME.2013.2281976.
[39] M. Xu, L. Chen, L. Zhang, H. Qi, L. Ma, J. Tang, B. Wan, and D. Ming, "A visual parallel-BCI speller based on the time–frequency coding strategy," *J. Neural Eng.*, vol. 11, no. 2, Apr. 2014, Art. no. 026014.
[40] M. Xu, J. Han, Y. Wang, T.-P. Jung, and D. Ming, "Implementing over 100 command codes for a high-speed hybrid brain-computer interface using concurrent P300 and SSVEP features," *IEEE Trans. Biomed. Eng.*, early access, Mar. 3, 2020, doi: 10.1109/TBME.2020.2975614.
[41] P. Lennie, "The cost of cortical computation," *Current Biol.*, vol. 13, no. 6, pp. 493–497, Mar. 2003.
[42] J. Chen, D. Zhang, A. K. Engel, Q. Gong, and A. Maye, "Application of a single-flicker online SSVEP BCI for spatial navigation," *PLoS ONE*, vol. 12, no. 5, May 2017, Art. no. e0178385.
[43] A. Maye, D. Zhang, and A. K. Engel, "Utilizing retinotopic mapping for a multi-target SSVEP BCI with a single flicker frequency," *IEEE Trans. Neural Syst. Rehabil. Eng.*, vol. 25, no. 7, pp. 1026–1036, Jul. 2017, doi: 10.1109/TNSRE.2017.2666479.

JIABEI TANG received the B.S. degree in biomedical engineering from Tianjin University, Tianjin, China, in 2013, where he is currently pursuing the Ph.D. degree. His research interests include biomedical signal processing and brain–computer interface systems based on steady-state visual evoked potentials.

MINPENG XU (Member, IEEE) received the B.S. and Ph.D. degrees in biomedical engineering from Tianjin University, in 2010 and 2015, respectively.

From 2014 to 2015, he visited the Tzyy-Ping Jung's Laboratory, Institute for Neural Computation, University of California at San Diego (UCSD), San Diego, CA, USA. He is currently an Associate Professor with the Department of Biomedical Engineering, Tianjin University. His research interests include brain–computer interface, neural signal processing, and neuromodulation techniques.

ZHENG LIU received the B.S. degree in biotechnology from Northwest A&F University, Yangling, China, in 2017, and the M.S. degree in biomedical engineering from Tianjin University, Tianjin, China, in 2020. His research interest includes application of deep learning in electroencephalogram processing.

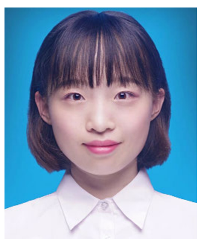

JINGJUAN QIAO received the B.S. degree in measurement and control technology and instrumentation from Henan University, Kaifeng, China, in 2019. She is currently pursuing the master's degree in biomedical engineering with Tianjin University. Her research interests include deep learning and its application in brain–computer interfaces.

SHUANG LIU received the B.S. degree in biomedical engineering from Tianjin Medical University, Tianjin, China, in 2012, and the M.S. and Ph.D. degrees in biomedical engineering from Tianjin University, Tianjin, in 2018.

She is currently an Assistant Professor with the Academy of Medical Engineering and Translational Medicine, Tianjin University. Her research interests include physiological mechanism of emotion, emotion recognition and regulation, and biomarker detection of the depression.

SHANGUANG CHEN received the B.S. degree from Wuhan University, Wuhan, China, in 1982, and the Ph.D. degree from the National University of Defense Technology, Changsha, China, in 2001. He is currently the Deputy Chief Designer with the China's Manned Space Program. His research interests include human factor engineering and aerospace medical engineering.

TZYY-PING JUNG (Fellow, IEEE) received the B.S. degree in electronics engineering from National Chiao Tung University, Hsinchu, Taiwan, in 1984, and the M.S. and Ph.D. degrees in electrical engineering from Ohio State University, Columbus, OH, USA, in 1989 and 1993, respectively. He is currently a Research Scientist and the Co-Director of the Center for Advanced Neurological Engineering, Institute of Engineering in Medicine, University of California at San Diego (UCSD), La Jolla, CA, USA, where he is also an Associate Director of the Swartz Center for Computational Neuroscience, Institute for Neural Computation, and an Adjunct Professor of bioengineering. He is also an Adjunct Professor of computer science with National Chiao Tung University, and an Adjunct Professor of the School of Precision Instrument and Opto-Electronic Engineering, Tianjin University, Tianjin, China. His research interests include biomedical signal processing, cognitive neuroscience, machine learning, electroencephalogram, functional neuroimaging, and brain–computer interfaces and interactions.

DONG MING (Senior Member, IEEE) received the B.S. and Ph.D. degrees in biomedical engineering from Tianjin University, Tianjin, China, in 1999 and 2004, respectively. From 2002 to 2003, he worked as a Research Associate with the Department of Orthopaedics and Traumatology, Li Ka Shing Faculty of Medicine, The University of Hong Kong. From 2005 to 2006, he was a Visiting Scholar with the Division of Mechanical Engineering and Mechatronics, University of Dundee, U.K. He joined the College of Precision Instruments and Optoelectronics Engineering, Tianjin University (TJU), as a Faculty Member, in 2006, where he has been promoted to a Full Professor of biomedical engineering, since 2011. He is currently the Head of the Neural Engineering and Rehabilitation Laboratory. His major research interests include neural engineering, rehabilitation engineering, sports science, biomedical instrumentation, and signal/image processing, especially in brain–computer interface, functional electrical stimulation, and gait analysis. He has been an International Advisory Board Member of the Foot, and the Editorial Committee Member of *Acta Laser Biology Sinica*, and the *International Journal of Biomedical Engineering*, China. He has managed over ten national and international research projects, organized and hosted several international conferences, as the Session Chair or Track Chair over the last ten years and was the General Chair of the 2012 IEEE International Conference on Virtual Environments, Human–Computer Interfaces and Measurement Systems (VECIMS 12). He is the Chair of the IEEE-EMBS Tianjin Chapter.